This article has been accepted for publication in a future issue of this journal, but has not been fully edited. Content may change prior to final publication. Citation information: DOI 10.1109/JESTPE.2017.2727978, IEEE Journal of Emerging and Selected Topics in Power Electronics



# Novel Maximum Electrical & Mechanical Power Tracking Controllers for Wind Energy Conversion Systems

Hassan Fathabadi

***Abstract*—Maximum power point tracking (MPPT) methods are currently implemented as maximum mechanical power trackers (MMPTs) in wind energy conversion systems (WECSs). In this study, the idea of a maximum electrical power tracker (MEPT) is first introduced. It is shown that the proposed MEPT extracts maximum output electrical power from a WECS, while a MMPT only extracts maximum mechanical power from the wind turbine used in the WECS. The novelties and contributions of this work are introducing the idea of a MEPT, and presenting two novel MEPT and MMPT having greater MPPT efficiencies and shorter convergence times compared to the state-of-the-art MPPT methods all implemented as MMPTs. Very simple structure, low-cost, and very good response to sudden variations in wind speed are the other advantages of utilizing the proposed MEPT and MMPT. A 600 W vertical wind turbine, a 1 kW DC/DC boost converter and a microcontroller have been used to construct the MEPT and MMPT, and experimental and simulation verifications are presented to validate theoretical results.**

***Index Terms*—Maximum electrical power tracker; maximum mechanical power tracker; maximum power point tracking; wind energy conversion system.**

## I. Introduction

A WECS essentially consists of a wind turbine and an electric generator [1], although an efficient WECS connected to a DC load also includes a three-phase rectifier, a DC/DC converter, and a MPPT controller [2]. A wind turbine is the key device of a WECS which converts wind energy into mechanical energy [3]. Nowadays, big wind turbines located in large wind farms are widely used to produce a portion of the electric power consumed in many countries [4]. Wind turbines are costly mechanical devices having low energy efficiency, so adopting an appropriate scheme to extract as much power as possible from WECSs is necessary [5]. At a certain wind speed, there is an optimum turbine speed at which the turbine output mechanical power reaches its maximum [6]. A MPPT controller tracks the optimum turbine speed, and then regulates the turbine speed to the optimum speed [7]. There are different MPPT methods reported in the literature [8] that are explained in detail as follows. Tip speed ratio (TSR) control is a well-known technique in which the turbine and wind speeds are continually measured by sensors or are estimated using different physical parameters. Moreover, the optimum TSR is also needed to regulate the TSR of the turbine to the optimum TSR [9]. Power signal feedback (PSF) control method needs the equation expressing the turbine output power or the maximum power curve of the turbine. This curve should be first obtained from off-line experiments or estimated by simulating. The turbine or wind speed is then used to extract the related maximum power from the mentioned power equation or curve to provide a reference power value for the MPPT controller [10]. Hill-climbing search (HCS) method, also known as perturb and observe (P&O) method, is an algorithm originally proposed for photovoltaic systems [11], it searches the maximum power of the turbine by perturbing the turbine speed [12]. The main drawback is that the algorithm convergency and tracking convergence time strictly depend on the current position of the turbine's operating point and the perturbation form, i.e., the algorithm may converge to wrong points [13]. Optimal torque control (OTC) method uses the mechanical torque equation or optimum torque curve to extract the turbine optimum torque associated with the current angular speed of the turbine [14]. Incremental conductance (INC) algorithm does not need any sensor, and uses the derivative of the power to track the MPP [15]. In a WECS, optimal-relation-based (ORB) algorithm uses an experimental or simulated curve representing the relationship between the turbine mechanical power and the DC current produced by the WECS to find the maximum mechanical power of the turbine [16]. The method does not need any speed sensor, but it has the disadvantages of the INC, OTC, and PSF control methods. Different fuzzy-based MPPT methods, which utilize fuzzy logic controls, have been reported in the literature [17]. The structure of such controllers is relatively complex but adaptive, so that, their parameters can be easily changed to increase the tracking accuracy and speed. In artificial neural network (ANN) MPPT methods, an ANN consisting of input, hidden, and output layers is first trained using actual data, the ANN is then used for MPPT [18].

In this work, the idea of a MEPT is introduced, and it is shown that in contrast with a MMPT, a MEPT extracts maximum output electrical power from a WECS. To prove this claim, two novel MEPT and MMPT having higher MPPT efficiencies and shorter convergence times compared to the state-of-the-art MPPT methods have been built. Very simple structure, low-cost, and very good response to sudden variations in wind speed are the other benefits of the two trackers. This paper is organized as follows. The implementation of the MMPT is explained in Section II. Similarly, the implementation of the MEPT is presented in Section III. Experimental and simulation results and energy efficiency analysis are presented in Section IV, and the study is concluded in Section V.

Hassan Fathabadi is an Associate Prof. at National Technical University of Athens (NTUA), Greece. Email: h4477@hotmail.com.

This article has been accepted for publication in a future issue of this journal, but has not been fully edited. Content may change prior to final publication. Citation information: DOI 10.1109/JESTPE.2017.2727978, IEEE Journal of Emerging and Selected Topics in Power Electronics



## II. Implementation of the Proposed MMPT

The schematic diagram of the WECS including the proposed MMPT is shown in Fig. 1. For the wind turbine used in the WECS, the tip speed ratio is defined as [19]:

$$\lambda = \frac{R\omega_m}{V_w} \quad (1)$$

where $V_w$ is the wind speed, $R$ and $\omega_m$ are respectively the radius and angular speed of the wind turbine. At a certain wind speed, the optimum angular speed $\omega_{m-opt}$, at which the maximum output mechanical power of the turbine occurs, can be obtained using (1) as:

$$\omega_{m-opt} = \frac{\lambda_{opt} V_w}{R} \quad (2)$$

where $\lambda_{opt}$ is the optimum tip speed ratio which is a specific parameter of a wind turbine. The circuit of the high-efficient DC/DC boost converter used in this study is shown in Fig. 2 [20]. The switch $S_1$ is a N-MOSFET which is switched with a constant switching period ($T_s$), where $T_s = 1/f_s$, and $f_s$ is the switching frequency. Duty ratio $D_{S1}$ is defined as $D_{S1} = t_{on}/T_s$, where $t_{on}$ is the switch on-time. The input resistance of the converter ($R_{in}$) is obtained as [20]:

$$R_{in} \approx \frac{(1-D_{S1})^2}{n^2} R_L \quad (3)$$

where $R_L$ is the load of the converter, and $n$ is the turns ratio of transformer $T$. As shown in Fig. 1, $I_{in} = k I_g$, where $k$ is a constant, $I_g$ is the output current of the permanent magnet synchronous generator (PMSG), and $I_{in}$ is the converter input current. It is deduced from (3) that the PMSG output current, and hence its rotor speed (turbine speed) can be controlled by varying the duty ratio $D_{S1}$. An increase in $D_{S1}$ causes a reduction in $R_{in}$, this increases $I_g$, and hence the braking electromagnetic torque induced by the PMSG ($T_L$). The increase in $T_L$ reduces $\omega_m$ according to the following equation expressing the dynamical behavior of the wind turbine:

$$T_m - T_L - f\omega_m = J\frac{d\omega_m}{dt} \quad (4)$$

where $J$ is the overall inertia of the system, $f$ is the viscous friction coefficient, and $T_m = \frac{P_m}{\omega_m}$ is the turbine torque, where $P_m$ is the turbine output mechanical power. Similarly, a reduction in $D_{S1}$ increases $\omega_m$. The experimental $\omega_m - D_{S1}$ curve of the constructed WECS is shown in Fig. 3. It can be summarized that $\omega_m$, and hence $\lambda$ can be regulated to the $\lambda_{opt}$ by varying $D_{S1}$ that is carried out by the proposed MMPT shown in Fig. 1. The proposed MMPT continually measures the wind speed using an anemometer, and calculates the associated optimum angular speed $\omega_{m-opt}$ using (2). The turbine angular speed is found from the angular frequency $\omega_e$ of the electric voltage produced by the PMSG as $\omega_m = \frac{\omega_e}{P}$.

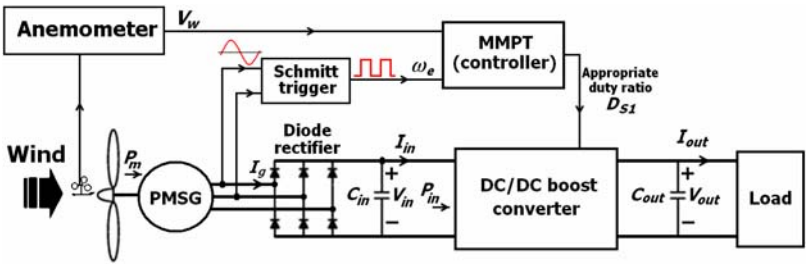


Fig. 1. Schematic diagram of the WECS including the proposed MMPT.

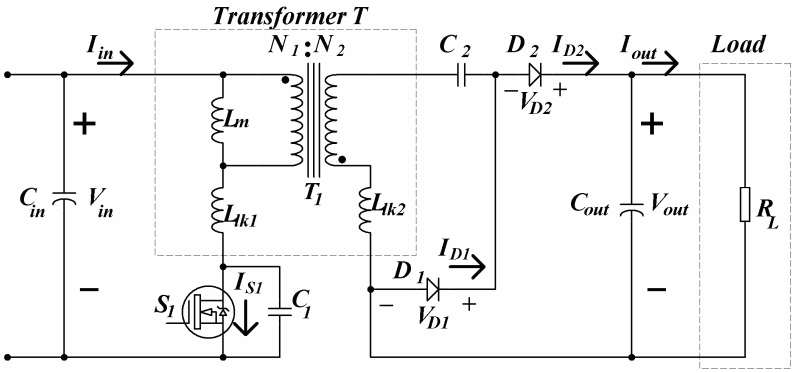


Fig. 2. DC/DC boost converter used in this study.

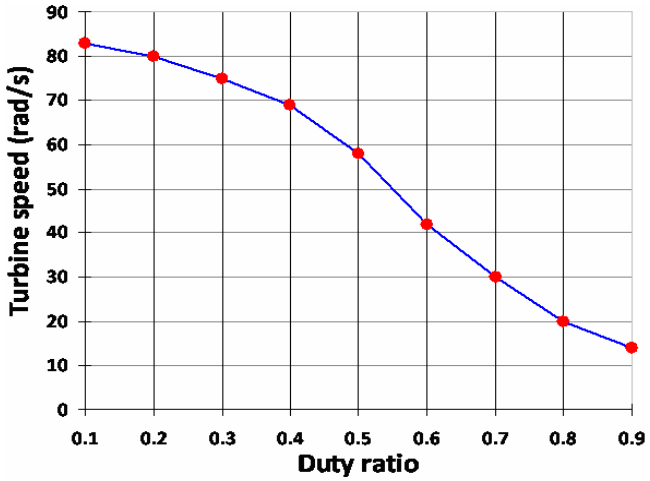


Fig. 3. Experimental $\omega_m - D_{S1}$ curve of the constructed WECS.

There are only three operation regions as below:

**Operation region 1:** If $\omega_m = \omega_{m-opt}$, there is no need to change $\omega_m$ by varying the converter duty ratio $D_{S1}$, so:

$$D_{S1}(k+1) = D_{S1}(k) \quad (5)$$

**Operation region 2:** If $\omega_m > \omega_{m-opt}$, the turbine speed should be reduced by increasing $D_{S1}$, so:

$$D_{S1}(k+1) = D_{S1}(k) + \Delta D_{S1} \quad (6)$$

where $\Delta D_{S1}$ is a positive value that will be explained next.

**Operation region 3:** If $\omega_m < \omega_{m-opt}$, the wind turbine speed should be increased by decreasing $D_{S1}$, so:

$$D_{S1}(k+1) = D_{S1}(k) - \Delta D_{S1} \quad (7)$$

The operational flowchart of the proposed MMPT is shown in Fig. 4. In this study, to minimize the tracking convergence time and maximize the MPPT efficiency, the amount of the

This article has been accepted for publication in a future issue of this journal, but has not been fully edited. Content may change prior to final publication. Citation information: DOI 10.1109/JESTPE.2017.2727978, IEEE Journal of Emerging and Selected Topics in Power Electronics



increase/decrease in $D_{S1}$ is selected based on the absolute value of the difference between the turbine angular speed and the optimum angular speed, i.e., $|\omega_m - \omega_{m-opt}|$. In fact, $\Delta D_{S1}$ is selected larger for the large amount of $|\omega_m - \omega_{m-opt}|$, and is selected smaller and smaller when $|\omega_m - \omega_{m-opt}|$ decreases. When $|\omega_m - \omega_{m-opt}|$ is large, the operating point of the wind turbine is far from the MPP, so a large increase/decrease in $D_{S1}$ is needed to rapidly move the operating point to around the MPP, and thus, $\Delta D_{S1}$ should be selected larger. In this study, $\Delta D_{S1}$ is selected as:

$$\Delta D_{S1} = \begin{cases} 0.100 & \text{when } |\omega_m - \omega_{m-opt}| \geq 20 \ rad/s \\ 0.010 & \text{when } 10 \ rad/s \leq |\omega_m - \omega_{m-opt}| < 20 \ rad/s \\ 0.005 & \text{when } 5 \ rad/s \leq |\omega_m - \omega_{m-opt}| < 10 \ rad/s \\ 0.002 & \text{when } 2 \ rad/s \leq |\omega_m - \omega_{m-opt}| < 5 \ rad/s \\ 0.001 & \text{when } 0 \ rad/s \leq |\omega_m - \omega_{m-opt}| < 2 \ rad/s \end{cases} \quad (8)$$

## III. Implementation of the Proposed MEPT

The schematic diagram of the WECS including the proposed MEPT is shown in Fig. 5. The PMSG output electric power $P_g$ can be expressed in the $(dq)$ reference frame as:

$$P_g = 3(v_d i_d + v_q i_q) \quad (9)$$

where $v_d$, $v_q$, $i_d$ and $i_q$ are the *d-q* output voltages and currents of one phase of the PMSG. $P_g$ can be obtained by subtracting the friction and copper losses from the turbine mechanical power as:

$$\begin{aligned} P_g &= P_m - 3R_s(i_d{}^2 + i_q{}^2) - f\omega_m{}^2 \\ &= C_p(\lambda) P_w - 3R_s(i_d{}^2 + i_q{}^2) - f\omega_m{}^2 \end{aligned} \quad (10)$$

where $C_p$ is the power coefficient of the turbine, and $R_s$ is the equivalent single-phase resistance of the stator. In this study, the turbine-generator power coefficient $C_{tg}(\lambda, \omega_m, i_d, i_q)$ evaluating the power efficiency of the wind turbine together with the coupled PMSG is defined as:

$$C_{tg}(\lambda, \omega_m, i_d, i_q) = \frac{P_g}{P_w} \quad (11)$$

where $P_w = 0.5\rho A V_w{}^3$ is the wind power, $\rho$ is the air density, and $A$ is the cross sectional area of the turbine. The turbine-generator power coefficient is obtained by using (10)-(11) as:

$$C_{tg}(\lambda, \omega_m, i_d, i_q) = C_p(\lambda) - \frac{3R_s(i_d{}^2 + i_q{}^2) + f\omega_m{}^2}{0.5\rho A V_w{}^3} \quad (12)$$

It is deduced from (12) that the turbine-generator power coefficient $C_{tg}(\lambda, \omega_m, i_d, i_q)$ and the turbine power coefficient $C_p(\lambda)$ reach their maximum values at different values of $\lambda$ due to the second term of the right side of (12) that depends on the turbine and wind speeds. Fig. 6 shows $C_p(\lambda)$ and $C_{tg}(\lambda, \omega_m, i_d, i_q)$ curves of the implemented WECS, when the wind speed is $6 m/s$. It can be seen that $C_p(\lambda)$ reaches its maximum at $\lambda_1 = \lambda_{opt}$ while $C_{tg}(\lambda, \omega_m, i_d, i_q)$ gets to its maximum at $\lambda_2$, where $\lambda_1 = \lambda_{opt} = 4.92$ and $\lambda_2 = 4.72$, and this explicitly validates the theoretical result presented by (12). Using Fig. 5, the converter input power $P_{in}$ supplied by the rectifier and filter capacitor is obtained as:

$$P_{in} = V_{in} I_{in} = P_g - P_{loss}(i_d, i_q) \quad (13)$$

where $P_{loss}$ is the rectifier power loss which depends on the PMSG output currents. The turbine-generator-rectifier power coefficient $C_{tgr}(\lambda, \omega_m, i_d, i_q)$ is defined as:

$$C_{tgr}(\lambda, \omega_m, i_d, i_q) = \frac{P_{in}}{P_w} \quad (14)$$

$C_{tgr}(\lambda, \omega_m, i_d, i_q)$ can be expressed in detail by substituting (13) in (14) as:

$$\begin{aligned} C_{tgr}(\lambda, \omega_m, i_d, i_q) &= \frac{P_g - P_{loss}(i_d, i_q)}{P_w} \\ &= C_{tg}(\lambda, \omega_m, i_d, i_q) - \frac{P_{loss}(i_d, i_q)}{0.5\rho A V_w{}^3} \end{aligned} \quad (15)$$

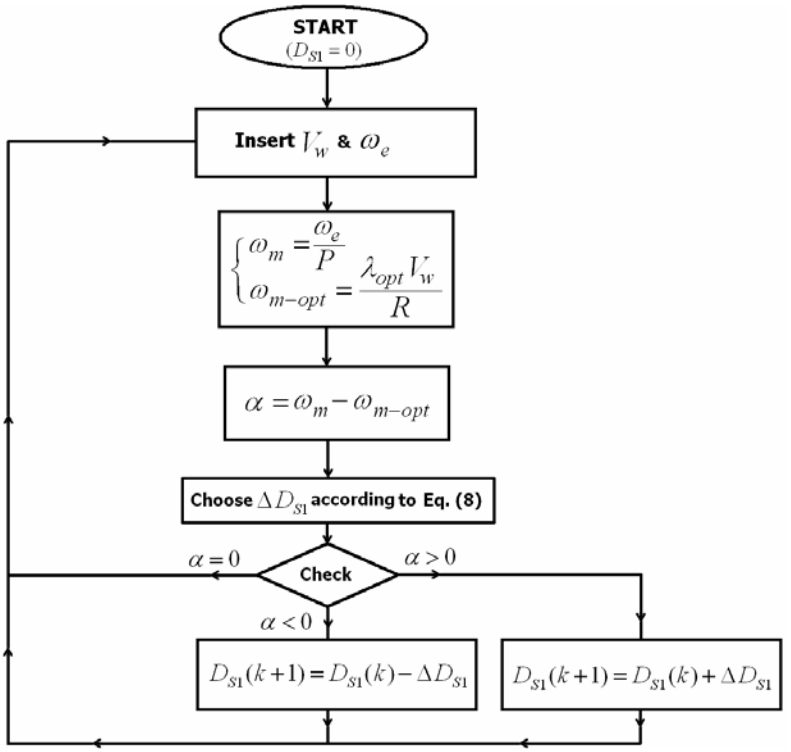


Fig. 4. Operational flowchart of the proposed MMPT.

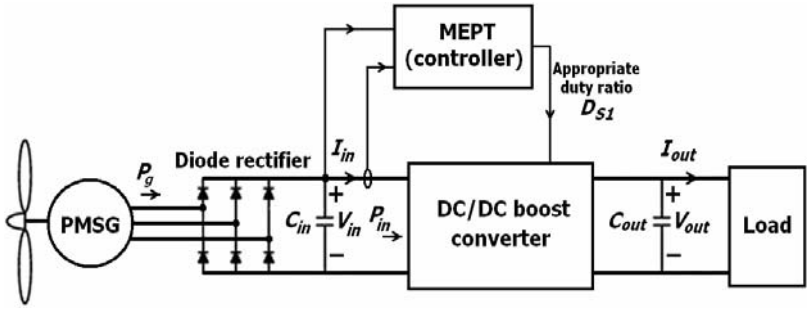


Fig. 5. Schematic diagram of the WECS including the proposed MEPT.

This article has been accepted for publication in a future issue of this journal, but has not been fully edited. Content may change prior to final publication. Citation information: DOI 10.1109/JESTPE.2017.2727978, IEEE Journal of Emerging and Selected Topics in Power Electronics



It is deduced from (15) that $C_{tgr}(\lambda,\omega_m,i_d,i_q)$ and $C_{tg}(\lambda,\omega_m,i_d,i_q)$ both reach their maximum values at the same value of $\lambda$ as shown in Fig. 6 because the second term of the right side of (15) only depends on the PMSG currents and the wind speed, i.e., it does not depend on the turbine speed. Fig. 6 shows that $C_{tgr}(\lambda,\omega_m,i_d,i_q)$ and $C_{tg}(\lambda,\omega_m,i_d,i_q)$ both get to their maximum values at $\lambda_2 = 4.72$ that verifies (15). It is clear that to extract as much power as possible from a WECS, $\lambda_2$ which maximizes $C_{tgr}(\lambda,\omega_m,i_d,i_q)$ should be tracked rather than $\lambda_1$ which maximizes $C_p(\lambda)$ because $\lambda_2$ maximizes the electric power supplied to the converter, while $\lambda_1$ only maximizes the output mechanical power of the wind turbine. Thus, the MMPT proposed in previous section tracks $\lambda_1$ while the MEPT presented in this section tracks $\lambda_2$ .Using (14), the converter input power can be expressed as:

$$P_{in} = P_w C_{tgr}(\lambda,\omega_m,i_d,i_q) = \frac{1}{2}\rho A V_w^3 C_{tgr}(\lambda,\omega_m,i_d,i_q) \quad (16)$$

So, at a certain wind speed $V_w$, the converter input power is a function of $\lambda$ obtained by only scaling $C_{tgr}(\lambda,\omega_m,i_d,i_q)$, i.e., $P_{in}$ and $C_{tgr}(\lambda,\omega_m,i_d,i_q)$ both get to their maximum values at $\lambda_2$. A typical $P_{in}-\lambda$ characteristic of the implemented WECS is shown in Fig. 7. The conditions that should be fulfilled on the different parts of the $P_{in}-\lambda$ curve are as follows. At the MPP $(\lambda_2, P_{in-\max})$: $\frac{dP_{in}}{dI_{in}} = 0$, at the left side of the MPP: $\frac{dP_{in}}{dI_{in}} < 0$, and at the right side of the MPP: $\frac{dP_{in}}{dI_{in}} > 0$.

The power slope $\alpha$ is defined as:

$$\frac{dP_{in}}{dI_{in}} \approx \frac{\Delta P_{in}}{\Delta I_{in}} = \alpha \; ; \quad when\ \Delta I_{in} \neq 0 \quad (17)$$

where $\Delta P_{in}$ and $\Delta I_{in}$ are respectively the deviations of the converter input power and current that are obtained as:

$$\begin{cases} \Delta I_{in} = I_{in}(k) - I_{in}(k-1) \\ \Delta P_{in} = V_{in}(k) I_{in}(k) - V_{in}(k-1) I_{in}(k-1) \end{cases} \quad (18)$$

where $V_{in}(k)$ and $I_{in}(k)$ are the k[th] samples of the converter input voltage and current when they are converted from analog to digital form. The flowchart showing the operation of the proposed MEPT is shown in Fig. 8. At first, the converter input voltage and current are sampled and read, then the MEPT calculates the deviations of the converter input power and current using (18). After that, the power slope $\alpha$ is computed using (17). Now, one of the following three conditions occurs:

1- If $\alpha = 0$ (at the MPP), there is no need to change $\omega_m$, so there is no need to vary $I_{in}$, and thus, $D_{S1}(k+1) = D_{S1}(k)$.

2- If $\alpha > 0$ (right side of the MPP), $\omega_m$ should be decreased by increasing $D_{S1}$ as $D_{S1}(k+1) = D_{S1}(k) + \Delta D_{S1}$.

3- Similarly, if $\alpha < 0$ (left side of the MPP), $\omega_m$ should be increased, by decreasing $D_{S1}$ as $D_{S1}(k+1) = D_{S1}(k) - \Delta D_{S1}$.

If $\Delta I_{in} = 0$, the MPPT controller returns to next loop and reads the next samples of the converter voltage and current.

The main criterion to select appropriate values for $\Delta D_{S1}$ is to reach a maximum value for the MPPT efficiency along with a minimum value for the tracking convergence time. When $|\alpha|$ is large, the operating point of the WECS is far from the MPP, so to minimize the tracking time, a large increase/decrease in $D_{S1}$ is needed to rapidly move the operating point to around the MPP, and thus, a larger amount of $\Delta D_{S1}$ should be selected. By approaching the MPP, $|\alpha|$ becomes smaller and smaller, so to maximize the MPPT efficiency, the increase/decrease in the converter input current should be smaller to exactly track the MPP, and thus, a smaller value should be chosen for $\Delta D_{S1}$. Considering the above explanation and noting the parameters of the implemented WECS, more than 65 experiments were performed by choosing different values for $D_{S1}$ that demonstrated selecting $\Delta D_{S1}$ according to the following role provides the highest MPPT efficiency along with the shortest tracking convergence time:

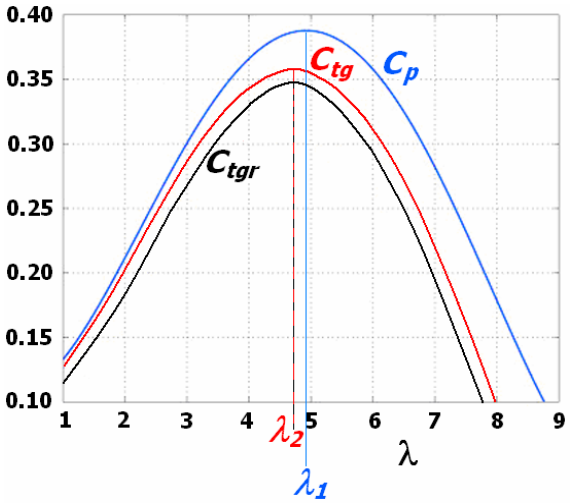


Fig. 6. $C_p(\lambda)$, $C_{tg}(\lambda,\omega_m,i_d,i_q)$, and $C_{tgr}(\lambda,\omega_m,i_d,i_q)$ curves.

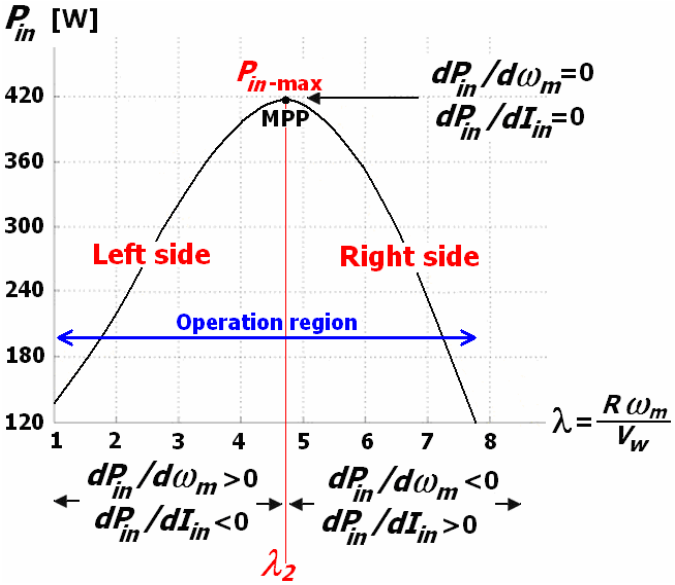


Fig. 7. Typical $P_{in}-\lambda$ characteristic of the WECS, $\lambda_2 = 4.72$.

This article has been accepted for publication in a future issue of this journal, but has not been fully edited. Content may change prior to final publication. Citation information: DOI 10.1109/JESTPE.2017.2727978, IEEE Journal of Emerging and Selected Topics in Power Electronics



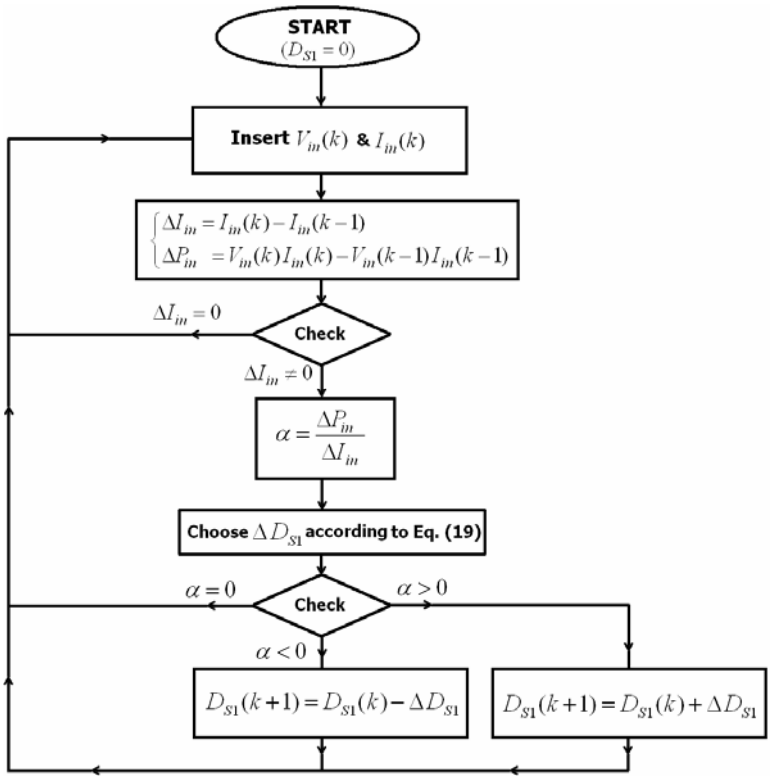


Fig. 8. Operational flowchart of the proposed MEPT.

$$\Delta D_{S1}=\begin{cases}0.100 & \text{when } |\alpha|\geq 10 \text{ W A}^{-1}\\ 0.010 & \text{when } 1 \text{ W A}^{-1}\leq|\alpha|<10 \text{ W A}^{-1}\\ 0.005 & \text{when } 0.5 \text{ W A}^{-1}\leq|\alpha|<1 \text{ W A}^{-1}\\ 0.001 & \text{when } 0 \text{ W A}^{-1}\leq|\alpha|<0.5 \text{ W A}^{-1}\end{cases} \quad (19)$$

The proposed MMPT and MEPT use the variable step-size duty cycles respectively defined by Eq. (8) and Eq. (19), so no oscillation around the MPP, diverging or even converging to an incorrect point occurs during the MPPT process.

## IV. Experimental and Simulation Results

In this section, experimental and simulation results associated with the proposed MMPT and MEPT are presented in three distinct sub-sections as follows.

### *A. MMPT: Experimental results*

Based on Fig. 1, a WECS has been built the electric circuit of which is shown in Fig. 9. A microcontroller MC68HC11A8 has been used to implement the MMPT. The flowchart shown in Fig. 4 has been applied to program the microcontroller. The three-phase output voltage of the PMSG is converted to the DC form using a three-phase diode bridge consisting of the six power diodes D3-D8 and the filter capacitor $C_{in}$. The output line voltage of the PMSG is decreased by the transformer $T_2$, and is supplied to an Op-Amp LTC 1047 which converts the input sine waveform to a square waveform with the angular frequency $\omega_e$. The square waveform is then supplied to pin 20 which is a bit-port of the microcontroller. An anemometer MAX 40+ has been used that needs a +24 V supply voltage, and produces 4-20 mA output current proportional to the wind speed. The anemometer output current is converted to a voltage in the range of 0-5 V using the potentiometer RV1, and is then supplied to pin 18 which is an analog/digital (A/D) pin of the microcontroller. The microcontroller extracts the angular frequency of the PMSG voltage ($\omega_e$) from the square waveform supplied to pin 20 using its internal timer, and measures the wind speed by sampling the voltage supplied to pin 18 with a sampling period of 100 $\mu s$. Then, the microcontroller produces an appropriate duty ratio $D_{S1}$ to track the MPP of the wind turbine. After that, the determined duty ratio $D_{S1}$ is supplied to the MOSFET switch $S_1$ as a periodic switching pulse with the duty cycle of $D_{S1}$ and a switching frequency ($f_s$) of 100 kHz through the transformer Trans-WE to regulate $\omega_m$ to $\omega_{m-opt}$. The optimum tip speed ratio of the wind turbine used in this study is 4.92 ($\lambda_{opt}=4.92$), and the experimental $P_m-\omega_m$ characteristics of the wind turbine for different wind speeds are shown in Fig. 10. The wind turbine was located in a wind tunnel, the constructed WECS was set up. At the wind speeds of 4 $m/s$, 6 $m/s$, 8 $m/s$ and 10 $m/s$, the output mechanical powers of the wind turbine extracted by the MMPT were measured using a shaft power meter SE110 made by Shoyo Engineering company. The output mechanical powers and the associated MPPT efficiencies are summarized in Table I. The experimental results reported in Table I demonstrate that the proposed MMPT has the MPPT efficiency of 98.04% at the rated wind speed (10 $m/s$).

TABLE I
MAXIMUM MECHANICAL AND ELECTRICAL POWERS EXTRACTED BY THE PROPOSED MMPT AND MEPT.

| Wind speed | Maximum available output mechanical power of the wind turbine (W) | Maximum available output electrical power of the WECS (W) | Maximum mechanical power of the wind turbine extracted by the MMPT (W) | Maximum output electrical power of the WECS extracted by | | MPPT efficiency of the MMPT (%) | MPPT efficiency of the MEPT (%) |
|---|---|---|---|---|---|---|---|
| | | | | MMPT (W) | MEPT (W) | | |
| 4 $m/s$ | 32.1 | 27.1 | 31.1 | 25.2 | 26.7 | 96.88 | 98.52 |
| 6 $m/s$ | 100.3 | 88.4 | 97.6 | 85.4 | 87.5 | 97.30 | 98.98 |
| 8 $m/s$ | 239.2 | 221.6 | 233.5 | 216.6 | 219.7 | 97.62 | 99.14 |
| 10 $m/s$ | 465.4 | 431.4 | 456.3 | 424.2 | 428.3 | 98.04 | 99.28 |

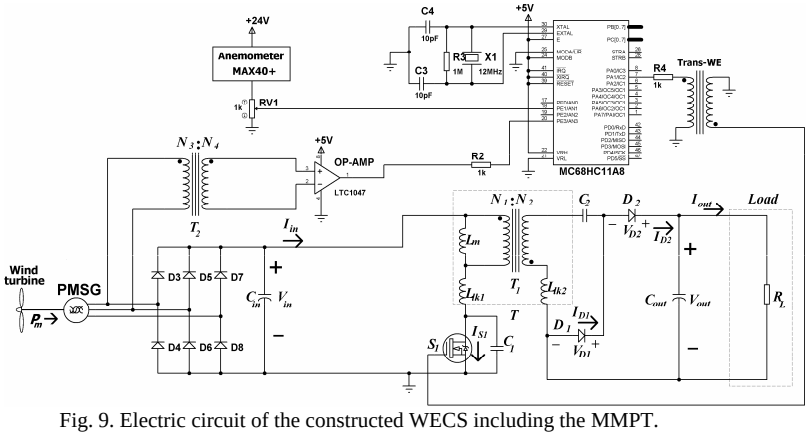


Fig. 9. Electric circuit of the constructed WECS including the MMPT.

This article has been accepted for publication in a future issue of this journal, but has not been fully edited. Content may change prior to final publication. Citation information: DOI 10.1109/JESTPE.2017.2727978, IEEE Journal of Emerging and Selected Topics in Power Electronics



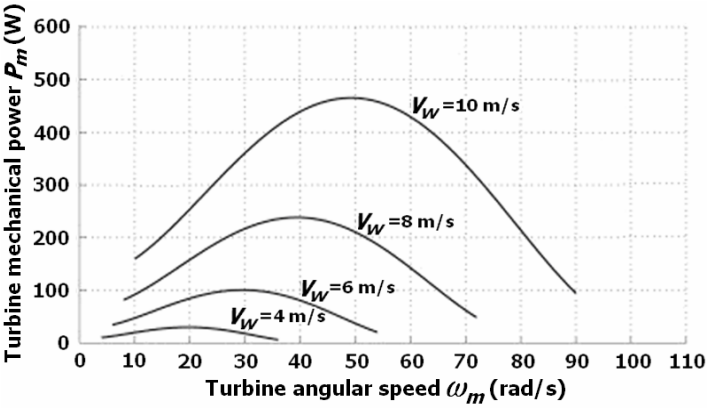


Fig. 10. Experimental $P_m - \omega_m$ characteristics of the wind turbine.

### *B. MEPT: Experimental results*

Based on the WECS shown in Fig. 5, a WECS including the proposed MEPT has been built. The electric circuit of the constructed WECS is shown in Fig. 11. A microcontroller MC68HC11A8 has been used to implement the MEPT. The flowchart shown in Fig. 8 has been utilized to program the microcontroller. The converter input current $I_{in}$ is continually measured by INA 168, and is supplied to pin 18 which is an A/D pin. The converter input voltage $V_{in}$ is first scaled by the potentiometer RV1, and then, is supplied to pin 17. The microcontroller continually samples the converter input current and voltage with a sampling period of 100 $\mu s$, and produces an appropriate duty ratio $D_{S1}$ to track the MPP of the WECS. After that, the determined duty ratio $D_{S1}$ is supplied to the MOSFET switch $S_1$ as a periodic switching pulse with a switching frequency of 100 kHz and the duty cycle of $D_{S1}$ through the transformer Trans-WE. At the wind speeds of $4\ ^m/_s$, $6\ ^m/_s$, $8\ ^m/_s$ and $10\ ^m/_s$, the output electrical powers of the WECS extracted by the MEPT and MMPT, and the MPPT efficiencies are reported in Table I. The experimental results reported in Table I verify that the proposed MEPT has the MPPT efficiency of 99.28% at the rated wind speed ($10\ ^m/_s$). It can be seen that the MEPT explicitly extracts more power compared to the MMPT. The experimental waveforms of the DC/DC boost converter of the MEPT at the rated wind speed are shown in Fig. 12, and the photo of the constructed WECS is also shown in Fig. 13.

## V. Conclusion

In this study, the idea of a MEPT was introduced. A MEPT was compared to a MMPT by constructing two novel MEPT and MMPT. It was shown that a MEPT extracts maximum electrical power from a WECS, while a MMPT only extracts maximum mechanical power from the wind turbine used in the WECS. The experimental and simulation verifications were presented, and the proposed MEPT and MMPT were also compared to the state-of-the-art MPPT methods. The experimental and simulation results together with the comparison explicitly demonstrated that the proposed MEPT and MMPT provide the highest MPPT efficiencies of respectively 99.28% and 98.04% along with the shortest convergence times of 15 ms and 18 ms compared to the state-of-the-art MPPT techniques. It was also deduced that the MEPT and MMPT not only provide very good responses to sudden variations in wind speed but also are simpler and lower-cost compared to the conventional ones, so that, the construction cost of the MEPT and MMPT is respectively 44 Euro and 132 Euro.

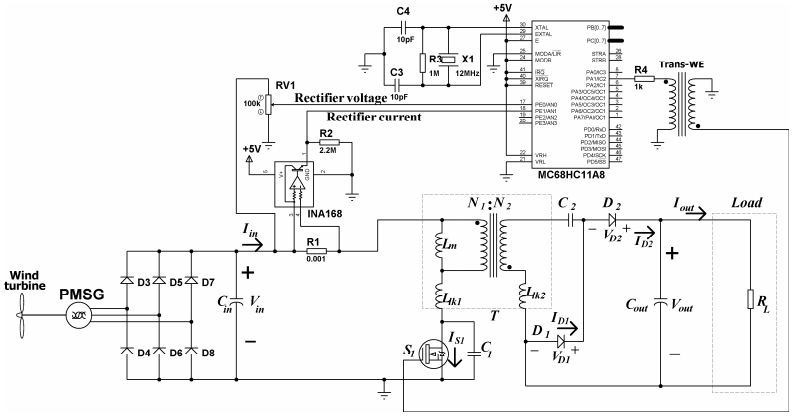


Fig. 11. Electric circuit of the constructed WECS including the MEPT.

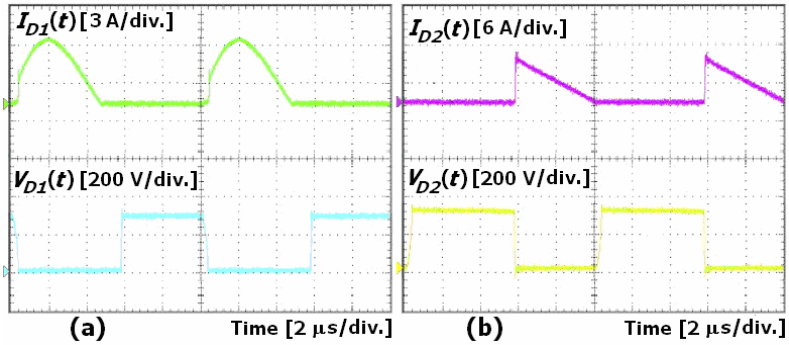


Fig. 12. MEPT: Experimental waveforms of the converter.

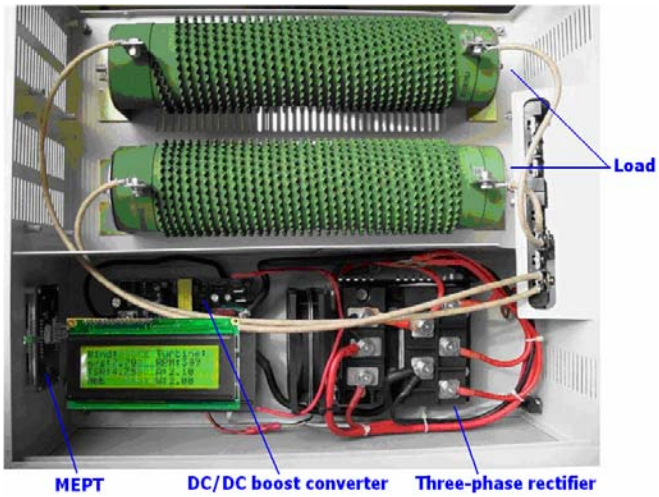


Fig. 13. Constructed WECS including MEPT.

## References

[1] H. Fathabadi, "Novel wind powered electric vehicle charging station with vehicle-to-grid (V2G) connection capability," *Energy Conversion and Management*, vol. 136, pp. 229-239, 2017.

[2] H. Polinder, J.A. Ferreira, B.B. Jensen, A.B. Abrahamsen, K. Atallah, and R.A. McMahon, "Trends in Wind Turbine Generator Systems,"

*IEEE Journal of Emerging and Selected Topics in Power Electronic*, vol.1, no.3, pp. 174-185, 2013.

[3] H. Fathabadi, "Control of a DFIG-based wind energy conversion system operating under harmonically distorted unbalanced grid voltage along with nonsinusoidal rotor injection conditions," *Energy Conversion and Management*, vol. 84, pp. 60-72, 2014.

[4] R.W. De Doncker and M. Ordonez, "Guest Editorial Special Issue on Distributed Generation," *IEEE Journal of Emerging and Selected Topics in Power Electronics*, vol. 5, no. 2, pp. 597-599, 2017.

[5] H. Fathabadi, "Novel grid-connected solar/wind powered electric vehicle charging station with vehicle-to-grid technology," *Energy*, vol. 132, pp. 1-11, 2017.

[6] H. Fathabadi, "Novel high-efficient unified maximum power point tracking controller for hybrid fuel cell/wind systems," *Applied Energy*, vol. 183, pp. 1498-1510, 2016.

[7] H. Fathabadi, "Novel highly accurate universal maximum power point tracker for maximum power extraction from hybrid fuel cell/photovoltaic/wind power generation systems," *Energy*, vol. 116, pp. 402-416, 2016.

[8] D. Kumar and K. Chatterjee, "A review of conventional and advanced MPPT algorithms for wind energy systems," *Renewable and Sustainable Energy Reviews*, vol. 55, pp. 957-970, 2016.

[9] H. Fathabadi, "Maximum mechanical power extraction from wind turbines using novel proposed high accuracy single-sensor-based maximum power point tracking technique," *Energy*, vol. 113, pp. 1219-1230, 2016.

[10] T. P. Chang, F. J. Liu, H. H. Ko, S. P. Cheng, L. C. Sun, and S. C. Kuo, "Comparative analysis on power curve models of wind turbine generator in estimating capacity factor," *Energy*, vol. 73, pp. 88-95, 2014.

[11] H. Fathabadi, "Novel fast dynamic MPPT (maximum power point tracking) technique with the capability of very high accurate power tracking," *Energy*, vol. 94, pp. 466-475, 2016.

[12] Q. H. Zhong, Y. Ruan, M. H. Zhao, and L. Tan, "Application of variable-step hill climbing searching in maximum power point tracking for DFIG wind power generation system," *Dianli Xitong Baohu yu Kongzhi/Power System Protection and Control*, vol. 41, no. 9, pp. 67-73, 2013.

[13] S. M. R. Kazmi, H. Goto, H. J. Guo, and O. Ichinokura, "A novel algorithm for fast and efficient speed-sensorless maximum power point tracking in wind energy conversion systems," *IEEE Trans. Industrial Electronics*, vol. 58, no. 1, pp. 29-36, 2011.

[14] K.-Y. Oh, J.-Y. Park, J.-S. Lee, and J. Lee, "Implementation of a torque and a collective pitch controller in a wind turbine simulator to characterize the dynamics at three control regions," *Renewable Energy*, vol. 79, pp. 150-160, 2015.

[15] K. Punitha, D. Devaraj, and S. Sakthivel, "Artificial neural network based modified incremental conductance algorithm for maximum power point tracking in photovoltaic system under partial shading conditions," *Energy*, vol. 62, pp. 330-340, 2013.

[16] Y. Xia, K. H. Ahmed, and B. W. Williams, "Wind turbine power coefficient analysis of a new maximum power point tracking technique," *IEEE Trans. Industrial Electronics*, vol. 60, pp. 1122-1132, 2013.

[17] V. Galdi, A. Piccolo, and P. Siano, "Designing an adaptive fuzzy controller for maximum wind energy extraction," *IEEE Trans. Energy Conversion*, vol. 23, pp. 559-569, 2008.

[18] R. Ata, "Artificial neural networks applications in wind energy systems: a review," *Renewable and Sustainable Energy Reviews*, vol. 49, pp. 534-562, 2015.

[19] W. Lingfeng, C. Singh, and A. Kusiak, *Wind Power Systems: Applications of Computational Intelligence*, New York: Springer, 2010.

[20] H. Fathabadi, "Novel high efficiency DC/DC boost converter for using in photovoltaic systems," *Solar Energy*, vol. 125, pp. 22-31, 2016.

**Hassan Fathabadi** was born in Tehran in 1969. He received the B.S., M.S., and Ph.D. degrees in electrical engineering from Tehran Polytechnic University, Iran, in 1992, 1997 and 2002, respectively.
From 2009 to 2012, he was a Postdoctoral Researcher with National Technical University of Athens, Athens, Greece, where he is currently an Associate Professor. He is the sole author of more than 55 papers published in high-ranking ISI journals and 15 inventions. His research interests include control, mechatronics, power electronics, energy and power systems.